



Engineering geological mapping of earthquake-induced landslides in South Lefkada Island, Greece: evaluation of the type and characteristics of the slope failures

N. Grendas¹ · V. Marinos¹ · G. Papathanassiou⁴ · A. Ganas² · S. Valkaniotis³

Received: 5 January 2018 / Accepted: 9 June 2018 / Published online: 18 June 2018
© Springer-Verlag GmbH Germany, part of Springer Nature 2018

Abstract

A moderate, shallow depth, earthquake ($M_w = 6.5$) occurred onshore Lefkada island on November 17, 2015 with the focal depth estimated at 11 km. The seismic fault is a near-vertical strike-slip fault running along the western coast, part of the Cephalonia Transform Fault. Landslides and ground cracks were mainly reported at the western part of the island, inducing structural damages. High severity slope failures occurred at Egremnoi and Gialos areas that both are located at coastal regions. This study aims to investigate the engineering geological conditions at these areas, and assess the characteristics and physical quantities (e.g., type, area— m^2 , and volume— m^3) of the instabilities. To achieve this, engineering geological mapping was implemented in Egremnoi and Gialos area aiming to; (a) classify the geological units mapped on the heavily damaged areas and (b) to correlate them with the type of slope failures. Furthermore, type and dimensions of slope failures were evaluated to estimate the total volume of the mass movement. All the data, originated from the engineering geological mapping, have been digitized and rasterized at 5 m grid spacing using the Arc/Info GIS software to perform a Newmark's sliding block analysis. The outcome arisen by this analysis is that the generated by the earthquake peak ground acceleration at these areas should be at least 0.45 g to trigger these kinds of slope failures.

Introduction

Landslides are one of the most collateral hazards related to earthquakes, inducing frequently exceeded damages directly related to strong shaking or fault ruptures (Jibson et al. 2000). Studying of earthquake-induced failures on regional scale is usually focused on the correlation of the seismic size (Magnitude- M) with basic parameters (Keefer 1984, 2002; Xu et al. 2014; Havenith et al. 2016), such as (1) the area affected by landslides due to the seismic event,

(2) the maximum distance of landslides from the earthquake epicenter, and (3) the maximum distance of landslides from the surface fault-rupture. As a preliminary approach, Keefer (1984) assessed that the smallest earthquake magnitude required to trigger slope failures is $M = 4.0$ for rock falls, rock slides, soil falls, and disrupted soil slides. From the other hand, according to Saroglou et al. (2017), the minimum earthquake magnitude in Greece for rockfalls is $M = 5.7$, while according to Papadopoulos and Plessa (2000), the relevant earthquake magnitude in Greece is $M = 5.3$.

Furthermore, taking into account the documentation of post-earthquake landslide spatial distribution, many researchers have highlighted the correlation between landslide distribution and topography. This statement was additionally strengthened by the fact that the strong ground motion is amplified in regions with steep morphology, while it is attenuated in valley-shaped regions (Jibson et al. 2000; Harp and Jibson 2002; Harp et al. 2014).

The last decade, several case studies of large-scale earthquake-induced landslides were documented and investigated in detail by scientists such as the 2008 Wenchuan, China earthquake ($M_w = 7.9$) that caused 197,481 landslides in area of 110,000 km^2 at the wider seismic affected area

✉ V. Marinos
marinosv@geo.auth.gr

A. Ganas
aganas@noa.gr

¹ Faculty of Sciences, School of Geology, Aristotle University of Thessaloniki, 541 24 Thessaloniki, Greece

² National Observatory of Athens, Institute of Geodynamics, Lofos Nymfon, 118 10 Athens, Greece

³ Koronidos 9, Trikala, Greece

⁴ Department of Civil Engineering, Democritus University of Xanthi, 67100 Kimmeria, Greece

(Shugen et al. 2013) and the 2011 off the Pacific coast of Tohoku Earthquake ($M_w=9.0$) that triggered a landslide in the vicinity of Aratozawa dam; the recorded PGA value was up to 1 g. In particular, this landslide produced 67 million cubic meters of material, and it is considered as one of the most disastrous landslides in Japan for the last 100 years (Miyagi et al. 2011). The 2010 Haiti earthquake ($M=7.0$) caused more than 7000 landslides southern of Port-au-Prince inside a 50 km buffer zone from the epicenter and along the southern coasts (Harp et al. 2013). Regarding Greece, the 2014 Cephalonia ($M_w=6.1$) and the 2015 Lefkada ($M_w=6.5$) events induced large-scale slope failures resulting to severe damages on road network (Valkaniotis et al. 2014; Papathanassiou et al. 2017).

Moreover, many researchers focus on the area affected by earthquake-induced landslides and aim to evaluate basic parameters (e.g., landslide area and volume, and landslide frequency) based on either post-earthquake survey or remote sensing techniques (Simonett 1967; Ohmori and Hirano 1988; Sasaki et al. 1991; Pelletier et al. 1997; Hovius et al. 1997). The volume of the triggered landslides is considered as more difficult to be quantified comparing to the total affected area (Malamud et al. 2004), due to the uncertainties dealing with the depth of each slope failure. For this purpose, many researchers have developed relations correlating the total failure areas with the relevant volume (Zekkos et al. 2017; Malamud et al. 2004; Hovius et al. 1997; Simonett 1967), while Harp and Jibson (1995) proposed mean depths for each type of landslides to obtain a deterministic-oriented approach.

This study focuses on one of the most active seismic zones in Europe, i.e., the island of Lefkada, which has been repeatedly struck by earthquakes through the last century (1911–2015). The surface magnitude (M_s) of instrumentally recorded earthquakes ranges between 5.3 and 6.4 (Papazachos et al. 2000; Papathanassiou et al. 2005, 2017). The main goal of this study is to correlate the engineering geological characterization of rock mass, assigned based on GSI classification, with the type and dimensions of the earthquake-induced landslides in two heavily damaged areas in south Lefkada, i.e., Egremnoi and Gialos regions, and to qualitative assess the landslide susceptibility for each engineering geological unit. Having documented these parameters, an evaluation of the total failure area, the mean landslide depth, and volume of slope failures was done. To achieve these goals, a field survey was conducted in July 2016 aiming to map in detail these areas on 1:3000 and 1:5000 scales.

It has to be underlined that a reliable and accurate estimate of the landslide volume could be performed based on data provided by geotechnical boreholes. However, no such data were available during this research. In addition, although the fact that we attempted to analyze aerial UAV-based information, it was not feasible to develop an accurate

model for the damaged areas due to very dense forest cover. The complexity of DEM construction using photogrammetry about areas with very dense forest cover has been solved with the usage of LIDAR technology. Many researchers have used this technology to construct landslide inventory maps (Jaafari 2018; Hasegawa et al. 2015; Chen et al. 2013; Eeckhaut et al. 2013; Ventura et al. 2013). However, LIDAR technology was not used during the field survey and similar corrections cannot be implemented here. From the other hand, Harp et al. (2011) mention that high-resolution satellite imagery is very useful for inaccessible areas but very expensive for resolutions less than 1 m. Accordingly, the landslide volume was estimated based on the published empirical relationships that were first introduced to evaluate erosion rate.

In addition, the classification of the rock mass in engineering geological units and the evaluated parameters of GSI for each unit were taken into account to assign a critical-acceleration value for these two sites by applying the Newmark's analysis (Jibson et al. 2000; Jibson 2007; Wang and Lin 2010; Papathanassiou 2012; Tang et al. 2013; Chung et al. 2014; Chen et al. 2014; Rodriguez-Peces et al. 2014; Wang et al. 2016; Liu et al. 2017; Vessia et al. 2017; Salinas-Jasso et al. 2017). In particular, the novelty of this study is that the parameters of geological formations such as c and φ are not assessed based on data collected from small-scale maps or based on information provided by the literature, but by taking into account the large-scale mapping and the evaluation of GSI per geological unit.

Geology and tectonic settings of the Lefkada earthquake

The geology of Lefkada Island has been studied by Bornovas (1964) and Cushing (1985), while the geological-tectonic framework has been extensively analyzed in the current literature (Rondoyanni et al. 2012; Papathanassiou et al. 2005, 2015; Ganas et al. 2016). The largest part of Lefkada belongs to the Ionian zone of the External Hellenides units, while Paxos zone is extended in the southwestern part of the island (Bornovas 1964; Cushing 1985). The lithostratigraphy mainly comprises carbonate formations of Ionian zone (Triassic-Jurassic) and of Paxos zone (Cretaceous and Oligocene). Ionian Flysch (Upper Eocene) that is mainly developed at the SE parts of the island, as well as with clastic Miocene sediments consisting of marls, limestones, and sandstones. Moreover, Pleistocene and Holocene deposits mainly occur in the northern part of Lefkada, and in Nydri and Vassiliki regions (Fig. 1).

In terms of tectonics, large elongated thrust and normal faults are observed, generally striking NNW–SSA (Mountrakis 2010); thrust faults striking NE–SW occur mainly

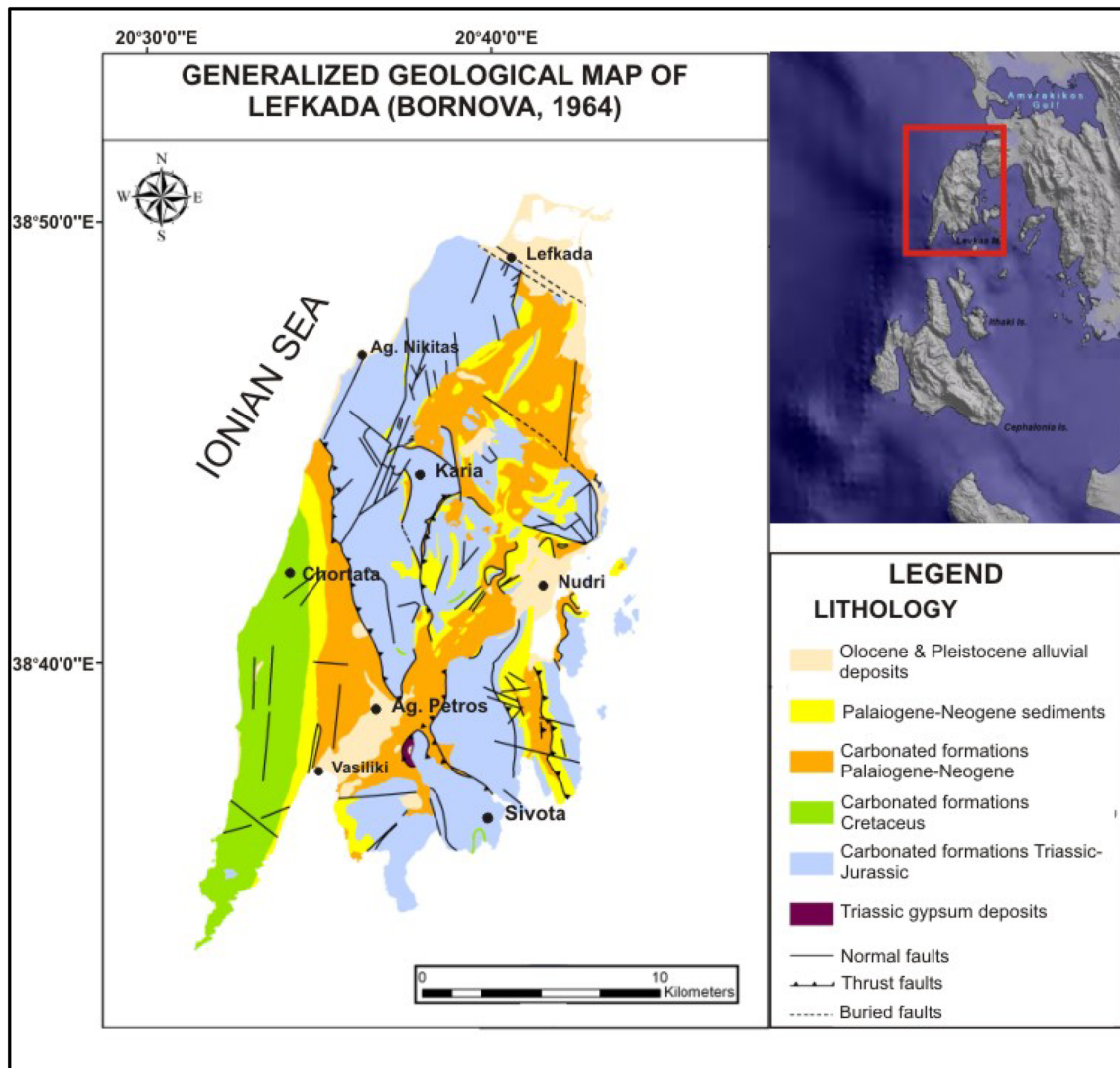


Fig. 1 Geological map of Lefkada is observed as it was mapped by I.G.M.E.—Institute of Geological and Mining Research (Bornovas 1964)

at the Ionian limestone (Bornovas 1964). Moreover, a normal fault system is observed with right lateral component trending NE–SW to NNE–SSW (Bornovas 1964) and minor normal faults trending NW–SE with left lateral component (Cushing 1985). Many of the ENE–WSW and N–S normal faults could be characterized as active faults, based on morphotectonic criteria (Papathanassiou et al. 2005, 2017). On the western part of the island and particularly, at the area where the two sites that are analyzed in this study are located, the tectonic regime is dominated by, the Athani-Draganos fault, that is the sub-parallel to the Cephalonia transform fault (CTF or KLTF). This is a NNE–SSW strike-slip fault dipping towards East and it is observed clearly in aerial photographs or satellite images (Papathanassiou et al. 2017). During its activation,

a system of normal faults was formed which acted during the Upper Pliocene–Upper Pleistocene (Cushing 1985).

The 2015 Lefkada earthquake-induced slope failures

The triggering factor of the landslides that are analyzed in this study is the $M_w = 6.5$ (focal depth 11 Km) moderate event that occurred on November 17, 2015 (7:10 GMT) (Ganas et al. 2016) (Fig. 2). The maximum PGA was 0.36 g, recorded at the seismological station of Vasiliki (ITSAK 2015).

Taking into account data provided by post-earthquake field surveys, it was concluded that the dominant

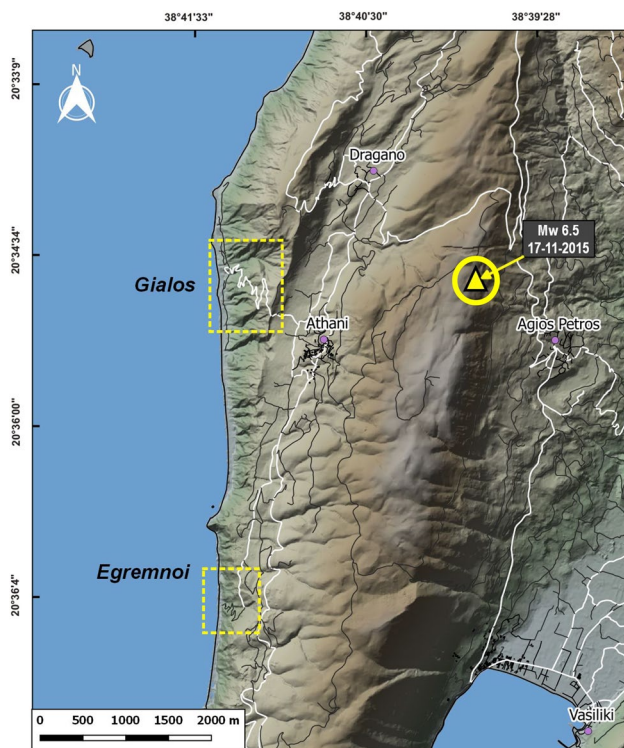


Fig. 2 Relief map of the southwestern part of Lefkada, showing the location of the sites where landslides are examined. Yellow sign marks the epicenter of the Mw 6.5 November 17, 2015 earthquake

geological effects triggered by the event were landslides and rockfalls that induced severe damages on the road network (Papathanassiou et al. 2017). These phenomena were mainly documented at the western part of the island, while their severity and density are decreased towards the eastern part (Lekkas et al. 2016; Zekkos et al. 2017; Papathanassiou et al. 2017).

The majority of slope failures, e.g., rock slides, debris flows, and shallow slides, were observed at Egremnoi and Gialos areas and along the 6 km road from the village Tsoukalades to Agios Nikitas (Papathanassiou et al. 2017). These areas consist of high slopes (> 150 m) with large dipping angles ($> 70^\circ$), while the rock mass consists of highly jointed limestone due to the tectonic regime as well as of debris material. In particular, at Egremnoi region, a deep landslide was reported affecting the paved road leading to the coast (Papathanassiou et al. 2017). The area called Gialos (Fig. 2) is located to the north of Egremnoi and has been also intensively damaged by the earthquake-induced slope failures.

Methodology

Engineering geological assessment of the rock mass

For the purpose of this study, a detailed geological–engineering geological mapping took initially place to report the lithology, tectonic structures, landslides, and engineering geological characteristics on the areas of interest. The documented data were collected and mapped at large scale (1:3000), while they were digitized and imported to the ArcGIS software (Fig. 5). The paths of the survey in both areas followed actually the pavement leading to the coast, while the slopes across the pavements were under investigation. The starting point for our investigation is referred as 0 + 000 (where the definition is km + meters). We divided each path into equally parts of 100 m by measuring the distance between the starting and ending point of each path (e.g. 0 + 000, 0 + 100.....1 + 000). The paths of the surveys can be seen in Figs. 5, 6, 7, and 14. In this way, it was adequately feasible to compile engineering geological units and easily yet effectively plot the reported information on the maps and import them to ArcGIS software.

Having mapped the geological units on both areas, an engineering geological characterization took place to assess and classify the rock mass as geotechnical entities, and to delineate units of similar engineering behavior. The former goal was achieved by applying well-known procedures focusing on the description and quantification of rock mass; (1) the GSI (Geological Strength Index) that represents the rock mass structure (Marinos and Hoek 2000), (2) the weathering degree (ISRM 1981), and (3) the Intact Rock Strength (IRS) (Hack and Huisman 2002) that represents the strength of intact rock pieces. Regarding the geological unit described as debris material, the engineering geological units are based on the difficulty of excavation with the geological hammer and on their cohesion as well. In particular, though the fact that the degree of excavation is not considered as a formal classification, it is widely accepted and used on field investigations for qualitative assessing of the debris material.

In particular, the GSI classification (Geological Strength Index), proposed by Marinos and Hoek (2000), is based on the evaluation of the rock mass structure and the condition of joint surfaces, and constitutes one of the existing classification systems as RMR (Bieniawski 1989) and Q (Barton et al. 1974) widely accepted. GSI classification system aims basically to the rock mass grading and defining geotechnical properties. Moreover, it is applicable in the case of heterogeneous rock masses (flysch and mollase). Taking into account that, at the areas of interest (Gialos, Egremnoi), the dominant geological formation is limestone, the relevant GSI system was used (Marinos 2010) (Fig. 3).

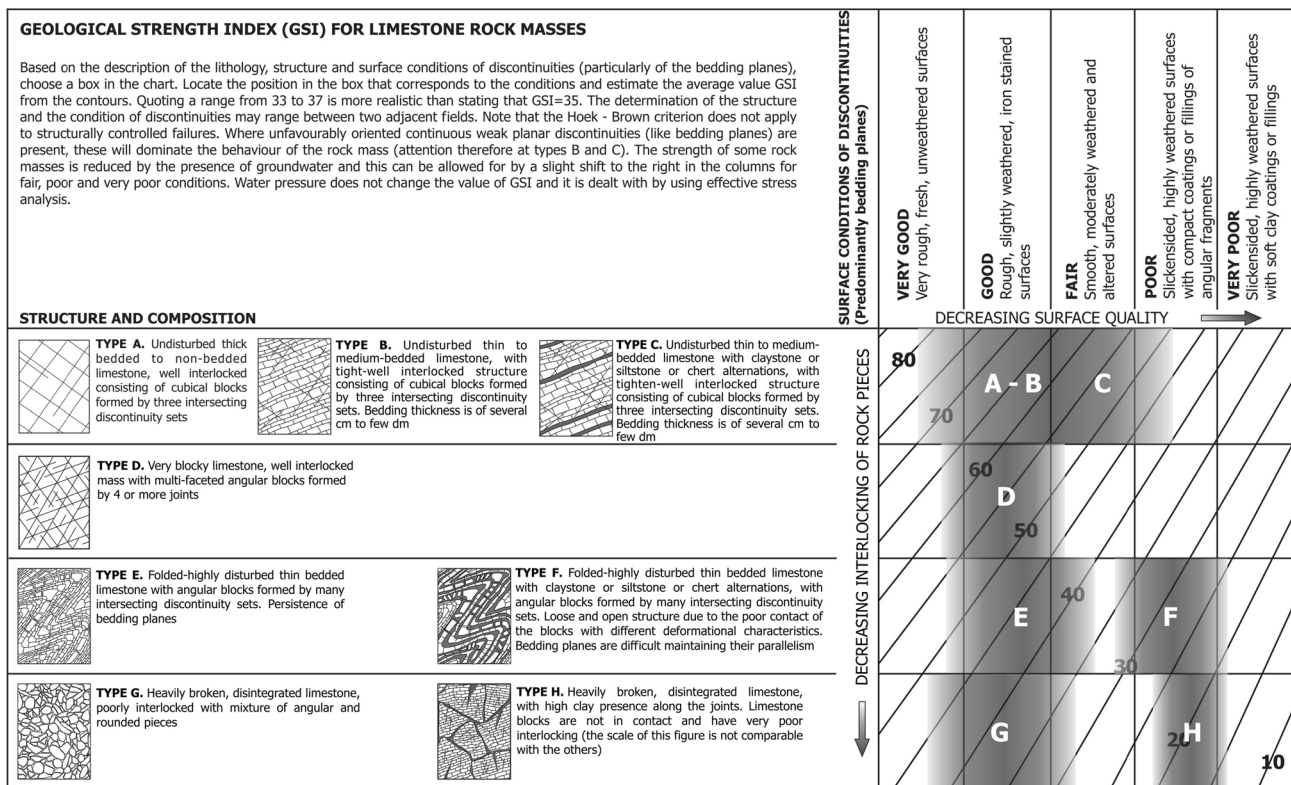


Fig. 3 GSI chart for limestone rock masses is observed (Marinos 2010)

One of the purposes of this research is to study the areas of interest in terms of the critical ground acceleration using Newmark’s analysis (Newmark 1965). Due to this fact, it is mandatory to calculate the friction angle (φ') and the cohesion strength (c') for each engineering geological unit using the Mohr–Coulomb parameters. The following equations, Eqs. (1) and (2), present the calculation method to extract friction angle (φ') and the cohesive strength (c') (Hoek 2006):

$$\varphi' = \sin^{-1} \left[\frac{6am_b(s + m_b\sigma'_{3n})^{a-1}}{2(1+a)(2+a) + 6am_b(s + m_b\sigma'_{3n})^{a-1}} \right], \quad (1)$$

$$c' = \frac{\sigma_{ci}[(1+2a)s + (1-a)m_b\sigma'_{3n}](s + m_b\sigma'_{3n})^{a-1}}{(1+a)(2+a)\sqrt{1 + 6am_b(s + m_b\sigma'_{3n})^{a-1}} / [(1+a)(2+a)]}, \quad (2)$$

where α , m_b , and s are parameters including GSI to be calculated and are given in Eqs. (3), (4) and (5); σ'_{3n} is given in Eq. (6).

It has to be noted that Eqs. (1) and (2) are applicable in the present study due to the fact that the regions of interest have been divided in engineering geological units. Each engineering geological unit is individual and it is partially independent of

the geological units, while it has different engineering geological parameters.

The following equations are used to determine the parameters used in Eqs. (1) and (2):

$$a = \frac{1}{2} + \frac{1}{6} (e^{-GSI/15} - e^{-20/3}), \quad (3)$$

$$m_b = m_i \exp \left(\frac{GSI - 100}{28 - 14D} \right), \quad (4)$$

$$s = \exp \left(\frac{GSI - 100}{9 - 3D} \right), \quad (5)$$

$$\sigma'_{3n} = \sigma'_{3max} / \sigma_{ci}, \quad (6)$$

$$\frac{\sigma'_{3max}}{\sigma'_{cm}} = 0.47 \left(\frac{\sigma'_{cm}}{\gamma H} \right)^{-0.94}, \quad (7)$$

$$\sigma'_{cm} = \sigma_{ci} \frac{[m_b + 4s - a(m_b - 8s)] (m_b/4 + s)^{a-1}}{2(1+a)(2+a)}, \quad (8)$$

where, GSI is the Geological Strength Index, D is a disturbance factor for the rock mass, σ'_{3max} is the upper limit of

the confining stress over which the relationship between the Hoek–Brown and the Mohr–Coulomb criteria is considered, σ_{ci} is the intact rock strength, σ'_{cm} is the rock mass strength, γ is the unit weight of the rock mass, and H is the slope height.

According to Hoek (2006), “Blast damage factor D is a factor which depends upon the degree of disturbance due to blast damage and stress relaxation. Applying the blast damage factor D to the whole rock mass is inappropriate and can result in misunderstanding and unnecessarily pessimistic results.” A small percentage of the regions of interest are pavements, while the major surface is unaffected by human influence. For this reason, it must be noted that, for all cases, $D=0$ is going to be used (i.e. it is assumed that no man-made disturbance or rock mass loosening due to agents acting on the surface of the ground).

Furthermore, to characterize the rock mass weathering degree, the ISRM (1981) weathering degree system was applied, where the rock mass is classified into six classes. Class “I” refers to healthy rock, while class “VI” refers to residual soil (Fig. 4). Below class II, rock mass with joints exists, while above class III rock mass with joints and soil exists. Thus, the rock mass quality is defined through the rock mass weathering degree.

The third parameter that was used to characterize the rock mass is the IRS classification system. IRS is considered as a reliable method to classify in situ the rock mass strength and it can be approximately related with the Unconfined Compressive Strength (UCS) (Table 1). It must be pointed out that more than one in situ tests have been implemented to achieve a reliable evaluation of rock mass strength following the suggestion of Hack and Huisman (2002).

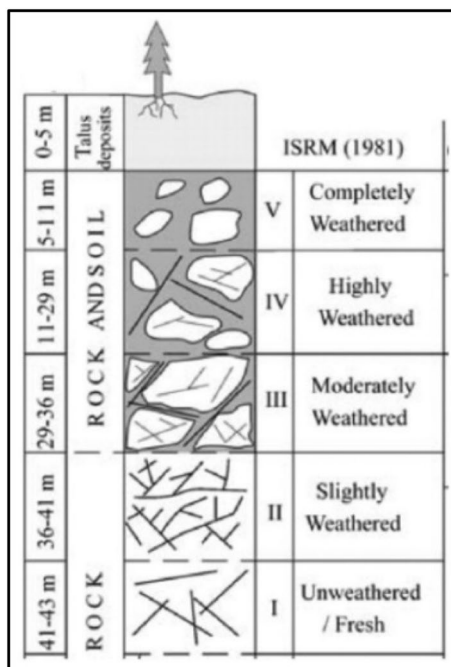


Fig. 4 Schematic perspective of weathering classification (ISRM 1981)

Evaluation of earthquake-induced slope failure characteristics

During the post-earthquake field survey, it was decided to classify the slope failures along the road network to attempt a correlation according to the type of failures with the engineering geological properties of the geological units. To achieve this, the classification proposed by Varnes (1978) was taken into account. This classification is mainly based on the nature of the material (rock and soil) and the movement type and secondarily on the material disturbance and the quantity of water which is contained in the material (Varnes 1978). Thus, the documented failures were classified as follows:

- *Shallow slides* Failures referring to sliding material with depth of sliding surface very close to the slope. The material is not defined and it could consist of intensely fractured or deformed rock mass, and in contrast, it could consist of debris material.
- *Deep-seated landslides* This kind of failures refers to exponentially large volume material movement with sliding surface greater than 5 m.

Table 1 Intact rock strength (IRS) classification compared with “simple means” test (Hack and Huisman 2002)

Intact rock strength (IRS) (MPa)	“Simple means” test (standard geological hammer of about 1 kg)	Description of material	Class
< 1.25	Crumbles in hand	Extremely weak	R0
1.25–5	Thin slabs break easily in hand	Very weak	R1
5–12.5	Thin slabs break by heavy hand pressure	Weak	R2
12.5–50	Lumps broken by light hammer blows	Medium strong	R3
50–100	Lumps broken by heavy hammer blows	Strong	R4
100–200	Lumps only chip by heavy hammer blows	Very strong	R5
> 200	Rocks ring on hammer blows. Sparks fly	Extremely strong	R6

- *Debris slides* Failures referring to the soil material (loose or dense, coarse, and fine).
- *Rock slides* The material of this kind of failures consists of intensely fractured or deformed rock mass.
- *Debris slides and Rock slides* It is a combination of those failures due to the fact that above the rock mass exists debris material.
- *Rock slides and Rock falls* The rock mass consists of intensely fractured or deformed rock mass, while in places, the fracture frequency of rock mass is lower and large blocks could be formed on a steep morphology.
- *Complex slides* These failures refer to every other failure that it could not be well defined due to complexity of its structure, while it is probably a combination of more than one of the pre-mentioned failures.

Furthermore, a qualitative-oriented assessment of the severity of these failures was realized by mainly taking into account the volume of the mass that failed and the percentage of the paved road that was covered by the sliding material defining the associated risk. The term severity was used to classify the reported earthquake-induced landslides by indirectly taking into account the amount of the material that moved downwards. It is a classification developed for the purposes of this study to facilitate the delineation of zones based on the consequences of slope failures. The goal of this classification is to correlate the severity to the parameters of the geological units and, as it is presented in the following sections, and to the triggering peak ground acceleration (PGA) based on Newmark's analysis. It should be pointed out that, in our approach, the Class "No Failure" does not employed to any area due to the fact that we were not present during the event, and accordingly, it was not feasible to precisely document that no failures zones exist, and to assign the "no failure" class to any of the geological units. Although the fact that this decision could be characterized as conservative, it was decided for the purposes of this study to avoid characterized an area as "no failure" by taking into account information provided by a field survey conducted few months after the triggering event. Unfortunately, aerial photographs could not accurately provide such information due to dense forest cover. The adopted qualitative-based classification is the following:

- *Low-to-very low severity* Areas where no failures or small-scale ones were documented during the field survey
- *Medium severity* Areas where the sliding material covered a very small part of the paved road
- *High severity* Areas where the sliding material covered half of the paved road
- *Extremely high severity* Areas where the sliding material extends for few meters and totally covers the paved road

Landslide volume estimation

An exertion was made to calculate the total volume (m^3) of the sliding material for both areas using the area affected by earthquake-induced landslides and multiplied with a mean depth for each type of landslides. Taking into account that the sliding surface is buried and heterogeneous, it was compulsory to apply mean depths for each type of landslide and after all to have a quite as possible approach of the mean sliding material volume (Malamud et al. 2004).

According to the literature, the mean depth of shallow slides ranges between 1 and 5 m, and the mean depth of deep-seated slides is > 5 m (Malamud et al. 2004; Harp and Jibson 1995). Amirahmadi et al. (2016) indicate that the mean depths of landslides observed in the area that they studied ranges from 2 to 5 m. In the present research, taking into account the—known from the literature—mean depths of shallow and deep-seated slides (essentially the maximum and minimum mean which could be observed), we made assessments about the mean depths of the observed failure types considering them as interpolated values. The classification of mean depths is presented in Table 2:

Many researchers in their studies have developed equations relating the failure area with the volume (Simonett 1967; Hovius et al. 1997; Malamud et al. 2004; Xu et al. 2016; Zekkos et al. 2017). These equations are extracted based on considerations of mean depths for each type of failure for the studied region. In this study, a comparison was made among the original (documented) volume estimations with functions taken from the literature. For the purposes of this study, two different equations were taken into account. The first equation had been extracted from a region with different geological conditions, while the second one was developed by taking into consideration data obtained from the whole Lefkada Island. Adopting this approach, a comparison among the pre-mentioned functions taken from literature with the volumetric results of the present study was implemented.

Table 2 Mean depth in meters for each failure type

Failure type	Mean depth (m)
Shallow slides	1
Rock slides	3
Rock slides and rock falls	3
Debris flows	2
Debris flows and rock falls	2
Deep-seated slides	6
Complex slides	5

In particular, Hovius et al. (1997) had studied the area and volume of landslides in Bewani and Torricelli Mountains in New Guinea, and developed the following power law equation in comparison with his results (Malamud et al. 2004):

$$V = \varepsilon \cdot A^{1.5}, \quad (9)$$

with V volume of landslides (m^3), A area affected by earthquakes (m^2), and $\varepsilon = 0.02\text{--}0.05$. Factor ε represents the volatility of volume (V) for different areas of interest.

It has to be underlined that to use Eq. (9), the authors choose to import an appropriate value ε for the maximum rendering of the referred equation. Consequently, the value ε is going to be equal to 0.05.

Simonett (1967) has also studied the same region and suggested the following power law equation:

$$V = 0.024 \cdot A^{1.368}, \quad (10)$$

with V volume of landslides (m^3) and A area affected by earthquakes (m^2).

Another important power law equation is derived by Xu et al. (2016). The studied area is Wenchuan, China, due to the 2008 earthquake ($M_w = 7.9$).

$$V = 1.0897 \cdot A^{1.2146}, \quad (11)$$

with V volume of landslides (m^3) and A area affected by earthquakes (m^2).

From the other hand, Zekkos et al. (2017) having studied the 2015 Lefkada earthquake-induced landslides have proposed the following power law equation:

$$V = 0.13 \cdot A^{1.4}, \quad (12)$$

with V volume of landslides (m^3) and A area affected by earthquakes (m^2).

The visualized results and comparisons can be seen in Figs. 10, 11, and 12. In Fig. 10, we can observe the volume ranges using the functions from the literature as well as the mean-depth method proposed by the authors. On the contrary, Figs. 11 and 12 represent a quantitative approach of the area (%) and volume (m^3) that each type of failure stands for.

Newmark's analysis

The development of a Newmark's analysis requires the evaluation of expected earthquake's shaking parameters and the capability of the geological units to resist this dynamic effect. The latter parameter is quantified as the critical acceleration (a_c), a threshold ground acceleration necessary to overcome basal sliding resistance and initiate permanent down slope movement (Jibson 2007). The computation of critical acceleration is based on the following equation proposed by Newmark (1965):

$$a_c = (\text{FS} - 1)g \sin \alpha, \quad (13)$$

where FS is the factor of safety, α is the angle of the sliding surface, and g is the acceleration of gravity.

The factor of safety is evaluated using a relatively simple limit-equilibrium model of an infinite slope in material having both frictional and cohesive strength (Jibson et al. 1998), and is given by the following:

$$\text{FS} = \frac{c'}{\gamma t \sin \alpha} + \frac{\tan \varphi'}{\tan \alpha} - \frac{m\gamma_w \tan \varphi'}{\gamma \tan \alpha}, \quad (14)$$

where φ' is the effective friction angle of rock mass, c' is the effective cohesive strength of rock mass, α is the slope angle, γ is the material unit weight, γ_w is the unit weight of water, t is the thickness of the mass at right angles to the slope, and m is the proportion of the slab thickness that is saturated (m is equal to 1 for saturated conditions and 0 for dry conditions).

The first fraction of the equation represents the cohesive component of the strength, the second fraction represents the frictional component, and the third fraction represents the reduction of the friction due to pore pressure (Jibson et al. 2000). Taking into account that Newmark's analysis is a regional scale procedure that is applied to indirectly assess the likelihood of slope failures, it is obvious that the pore water pressure per site and locality cannot be evaluated. Therefore, the values of c' and φ' were computed based on Eqs. 3 and 4.

The Newmark analysis can be extended to regional analysis using the GIS software (Miles and Keefer 2000), Arcinfo, by applying Eqs. (1) and (2) to raster data layers created for each input variable.

Having computed the factor of safety, Eq. (14), the next step was the estimation of the critical acceleration using Eq. (13). Following the recommendation of Jibson et al. (1998), areas (pixels) where the value of factor of safety $\text{FS} < 1$ have been reordered as $\text{FS} = 1.01$ to be on stable conditions before the earthquake occurrence. The compiled critical-acceleration map can be characterized as a seismic landslide susceptibility map as it delineates areas prone to slope failure independent of any ground-shaking scenario (Jibson et al. 1998) (Tables 3, 4).

Results

Geological mapping

The areas of interest consist entirely of Paxos zone materials and the rock masses comprise carbonate formations mainly limestone.

Table 3 Engineering geological units for Egremnoi area

Engineering GEOLOGICAL Units “Egremnoi”									
A/A	GSI	Weathering	Strength	Slope inclination	Slope height (m)	Excavation with geological hammer	Cohesion	Failure type	Comments
Engineering geological unit 1	60–70	I–II	R5–R6	80°–85°	5–50	–	–	No failure	–
Engineering geological unit 2	55–60	II	R5	80°–85°	5–10	–	–	Rock slides and rockfalls	Failures occurred only for a small area
Engineering geological unit 3	35–45	II	R4	35°–40°	10–20	–	–	No failure	Folded rock mass
Engineering geological unit 4	25–30	III	R3	35°–40°	5–20	–	–	Rock falls—deep slides	–
Engineering geological unit 5	15–20	III–IV	R2–(R1)	45°–50°	5–30	Easy	–	Rock slides and rockfalls	–
Engineering geological unit 6	–	–	–	60°–70°	7–10	Easy	Loose	Debris flow—rock falls	–
Engineering geological unit 7	–	–	–	50°–60°	6–10	Difficult	Strong	Surface slides	Potential failures due to rainfall

Table 4 Engineering geological units for Gialos area

Engineering Geological Units “Gialos”									
A/A	GSI	Weathering	Strength	Slope inclination	Slope height (m)	Excavation with geological hammer	Cohesion	Failure type	Comments
Engineering geological unit 1	60–70	II	R5	> 70°	5–10	–	–	No failure	The limestone bedding is observed
Engineering geological unit 2	55–60	II–III	R4–(R3)	45°–50°	15–20	–	–	Rock slides and rockfalls	–
Engineering geological unit 3	35–45	III	R3	60°–70°	6–10	–	–	Rock slides and rockfalls (deep slides)	–
Engineering geological unit 4	15–20	IV	R2–(R1)	40°–45°	3–10	–	–	Rock slides, rockfalls, deep slides	–
Engineering geological unit 5	–	–	–	45°–50°	6–10	Easy	Loose	Debris flow	–
Engineering geological unit 6	–	–	–	60°–70°	6–10	Difficult	Strong	No failure	Same behavior as geo-technical unit 1

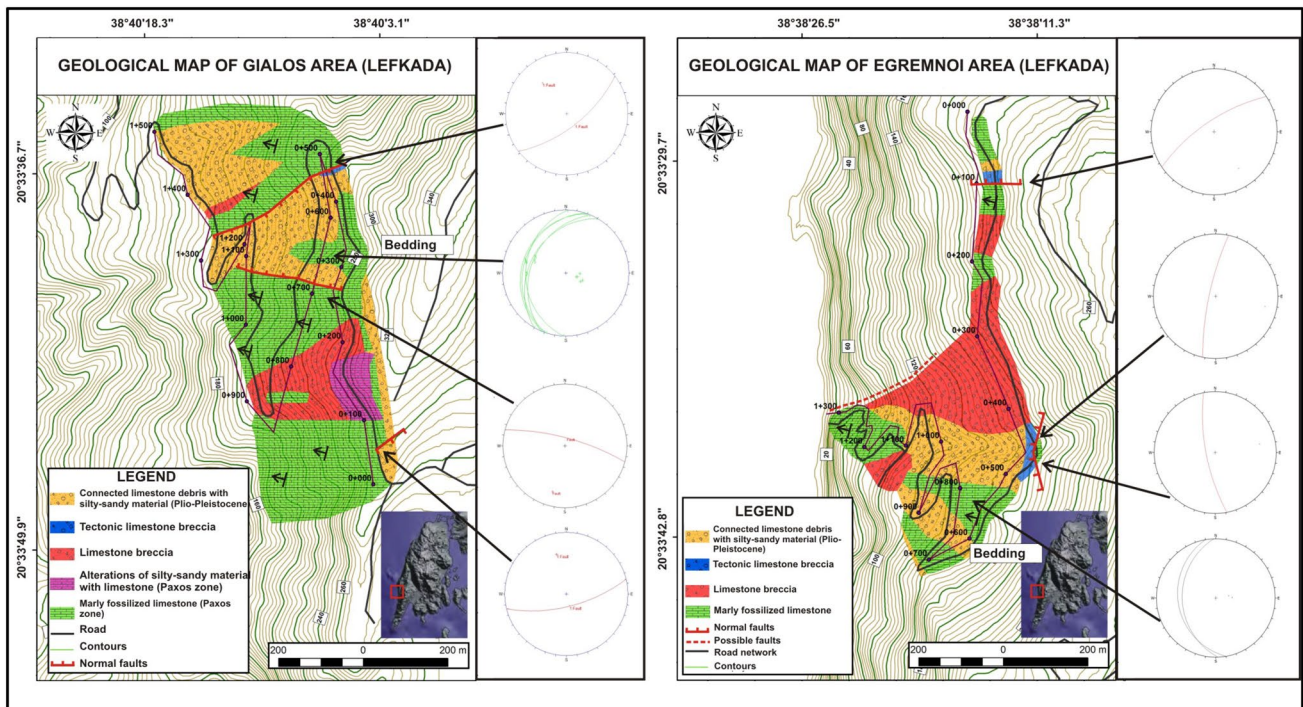


Fig. 5 Geological maps constructed by the field investigation. Geological map of Gialos area (left) and geological map of Egremnoi area (right)

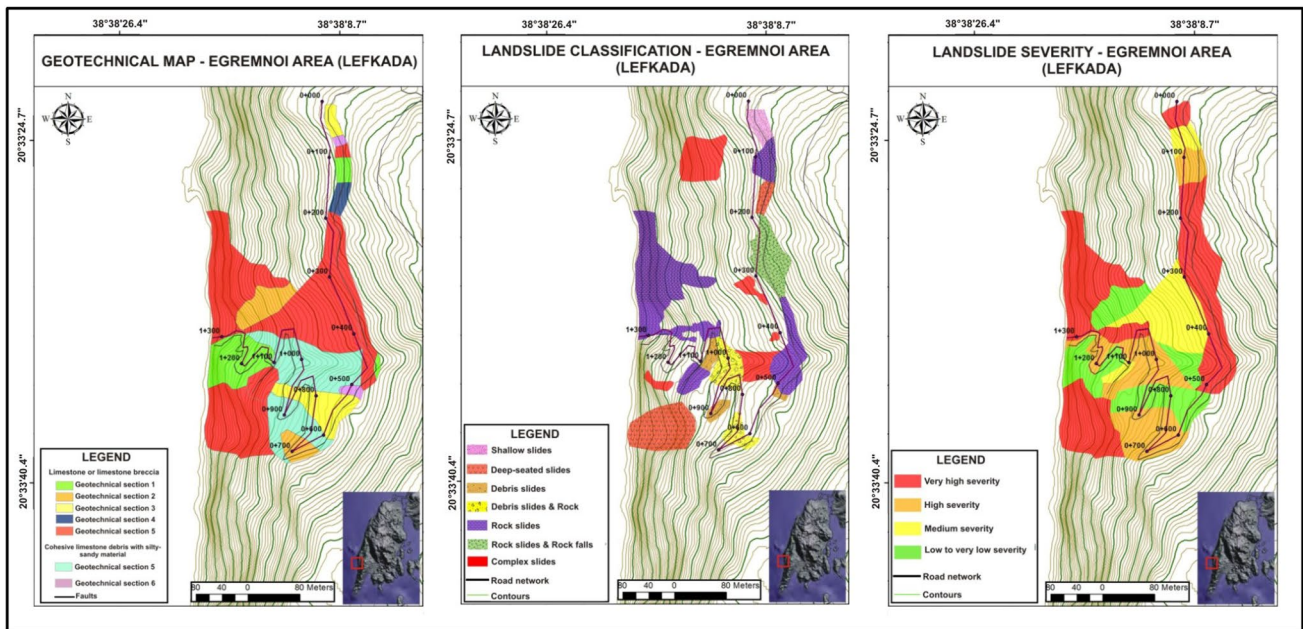


Fig. 6 Thematic maps for Egremnoi area. a Engineering geological map including engineering geological units (left), b landslide classification map according to Varnes (1978) (centre), and c landslide severity map (right)

Gialos area

According to Bornovas (1964), the Gialos area consists of limestone with ammonites of Paxos zone (Upper Jurassic)

as bedrock. In some locations, the same limestone appears as breccia. A transition of limestone-to-clastic material was observed, an evidence of a local difference in sedimentation. In the same area, two (2) normal faults exist and they have

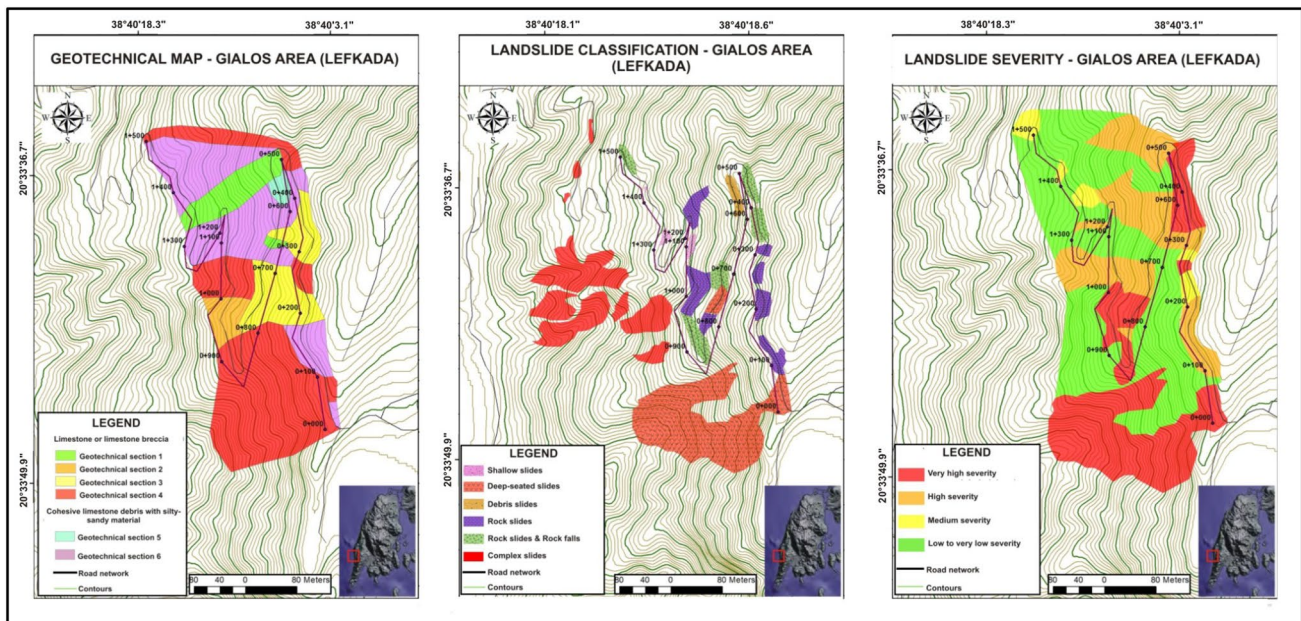


Fig. 7 Thematic maps for Gialos area. **a** Engineering geological map including engineering geological units (left). **b** Landslide classification map according to Varnes (1978) (centre). **c** Landslide severity map (right)

formed a small tectonic graben which contains debris and brecciated limestone (Fig. 5).

Egremnoi area

According to Bornovas (1964), the Egremnoi area consists of layered limestone of Paxos Zone (Upper Cretaceous), (Fig. 5). It is either well welded or loose limestone thick and layered. The existence of bedding in carbonate debris is related to the chronic sedimentation of a river and flood deposits. Limestone breccia related to a normal fault zone is also found covering a significant area.

Engineering geological mapping

Regarding the general engineering geological conditions of the areas of interest, the bedrock (limestone) is mainly deformed due to the intensive tectonic regime. Limited are the cases where the bedrock is massive with high strength and with no observed failures. In most cases, the bedding of the bedrock is deformed and difficult to detect and measure. It is of major importance that no kinematic failures occurred, since there is no existence of joint sets with high persistence. The limestone debris of the areas, although it is mainly connected with high cohesive strength, present also loose parts with low-to-medium cohesive strength.

Egremnoi area

The engineering geological mapping was implemented up to 1 + 300 m along the paved road due to the fact that the failures stopped occurring approximately at this point. As it is shown in Fig. 6 in comparison with the Fig. 5b, the limestone breccia appears as the most deformed (Engineering geological unit 4 and 5, depending on the rock mass quality) and this is the unit which caused the major sliding material (rock sides, rock falls, and deeper seated slides), while the severity is characterized as high-to-very high. On the contrary, the intact limestone which is observed mainly near the coast belongs to engineering geological unit 1 and caused no or very few failures (low-to-very low severity). Geological unit 7 has the same behavior to engineering geological unit 1 which refers to the limestone debris with high cohesive strength. Engineering geological unit 2, 3, and 6 caused mainly complex slides, rock falls, and debris flows, while the landslide severity is characterized as medium. Typical photographs of each engineering geological unit are presented in Fig. 8.

Gialos area

The engineering geological mapping was implemented up to 1 + 500 m along the pavement due to lack of observed failures at this point and beyond. In Fig. 7 in comparison with the Fig. 5a, we can observe that it is not only the limestone breccia that appears as the most deformed yet is the limestone bedrock with the same

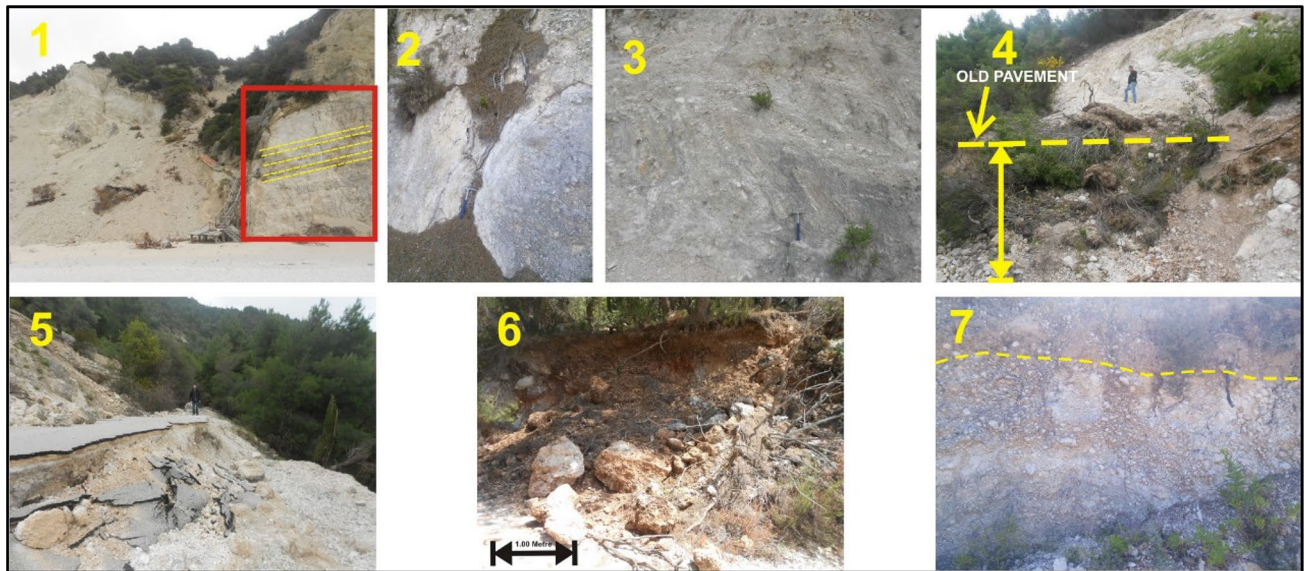


Fig. 8 Field photographs from Egremnoi area representing each engineering geological unit. The photographs were taken on July 11, 2016 by the authors. The numbers represent each engineering geological unit

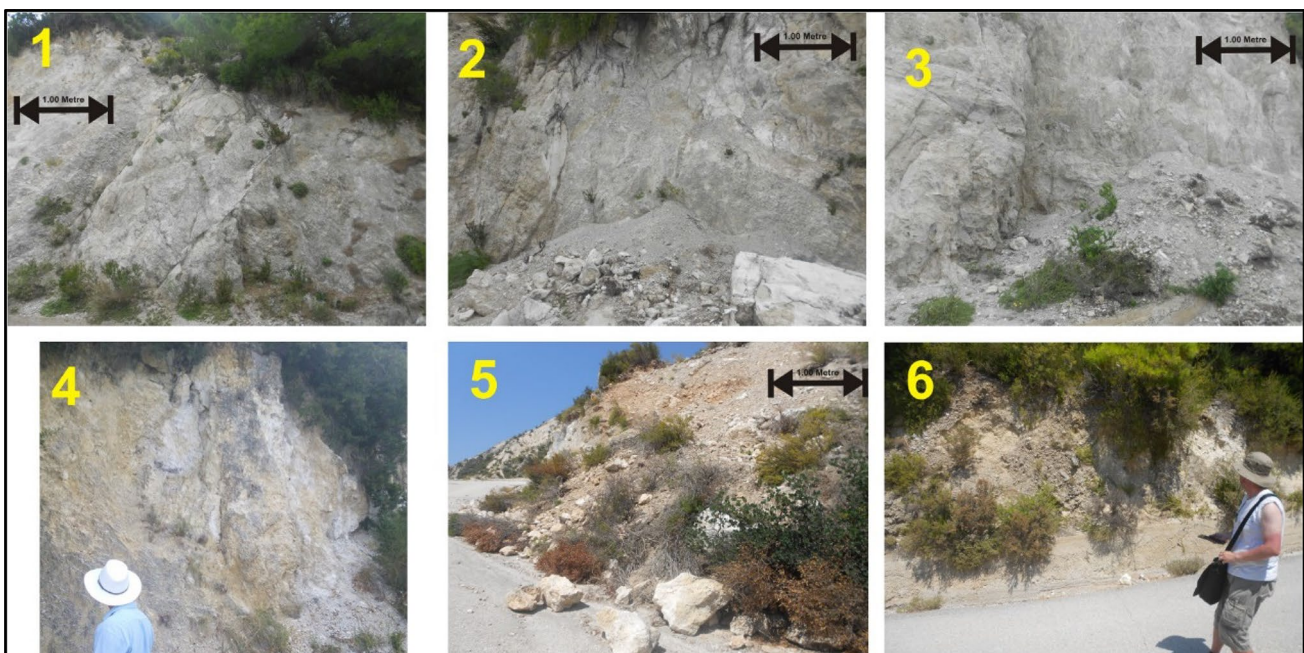


Fig. 9 Field photographs from Gialos area representing each engineering geological unit. The photographs were taken on July 13, 2016 by the authors. The numbers represent each engineering geological unit

deformation due to weathering (Engineering geological unit 3 and 4, depending on the rock mass quality). These engineering geological units caused the major sliding material (rock sides, rock falls, deeper seated slides, and complex slides), while the severity is characterized

as high-to-very high. The intact limestone is observed mainly at the western part of the area which belongs to engineering geological unit 1. This engineering geological unit caused no or very few failures (low to very low severity). The same behavior to engineering geological

Fig. 10 Volume range for Egremnoi and Gialos regions using the mean-depth method and two bibliographical equations

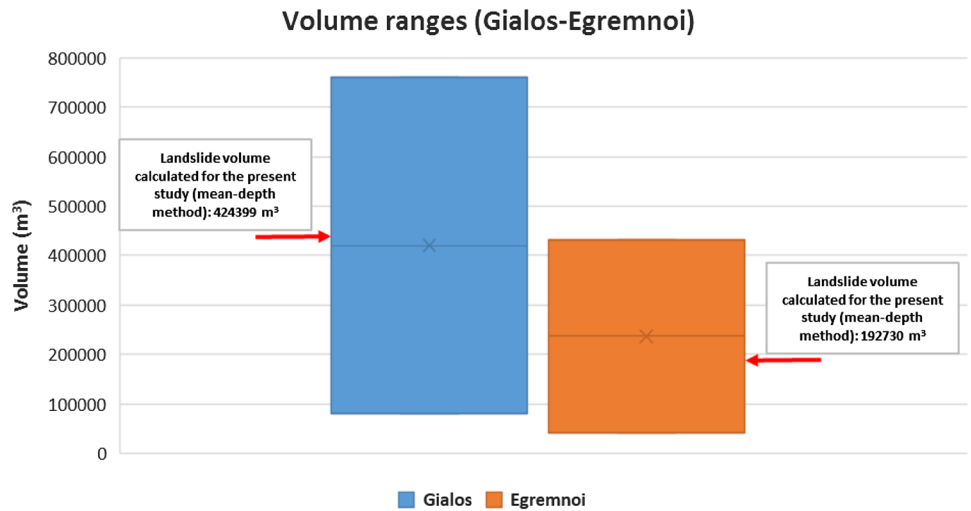


Fig. 11 Area percentage (%) and total volume (m³) for each type of landslide for Gialos area

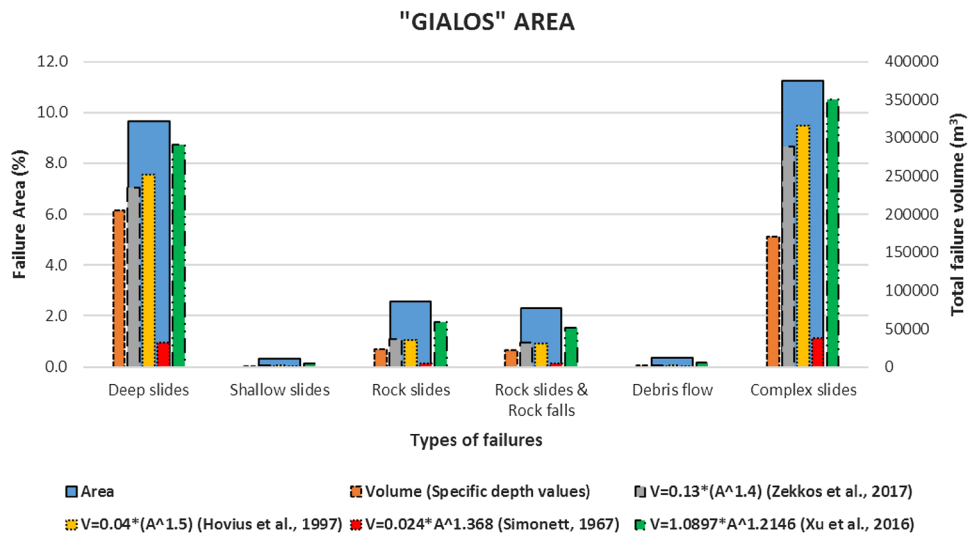
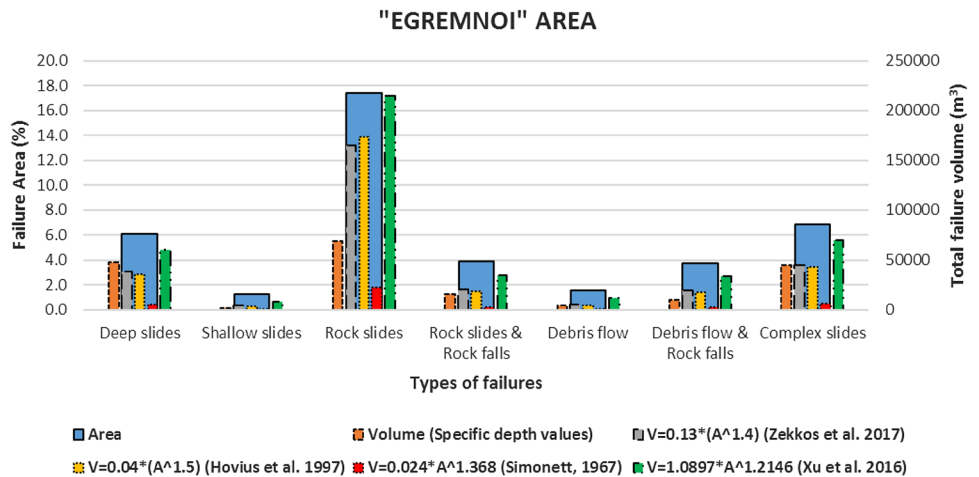


Fig. 12 Area percentage (%) and total volume (m³) for each type of landslide for Egremnoi area



unit 1 has the engineering geological unit 6 which refers to the limestone debris with high cohesive strength. Engineering geological unit 2 and 5 caused mainly rock slides and rock falls and limited debris flows, while the landslide severity is characterized as medium (Fig. 8). Typical photographs of each engineering geological unit are presented in Fig. 9.

Failure area percentage and total volume estimation

The compilation of the landslide classification map for each area is obviously a tool to visualize the failure types, and additionally to assess the failure area (m^2) and the relevant volume per slope failure class. We assessed the total failure area (including all type of landslides) and the failure area per each type of landslide for both regions, respectively. The study area of Gialos area is equal to 0.3 km^2 and the study area of Egremnoi area is equal to 0.13 km^2 . Taking into account the spatial distribution of slope failures, shown in Figs. 6b and 7b, and the assumption presented in the chapter of “Methodology” regarding the mean depth of failures, the area percentage (%) and total volume (m^3) for each type of landslide for Egremnoi and Gialos regions are estimated and presented in Figs. 11 and 12, respectively.

In particular, the sum of volume of sliding material for Gialos and Egremnoi areas—using the estimated mean depths—is equal to 424,399 and $192,730 \text{ m}^3$, respectively. Taking into account the equations Eqs. (9), (10), (11), and (12), the sum of volume of sliding material was additionally estimated concluding that the volumetric results are higher than the relevant ones arisen by mean depth method. It has to be underlined that the slope failures that were identified relate to multiple landslide masses and exist entirely in the areas of interest. Based on Eq. (9), the estimated sum of volume for Gialos and Egremnoi area is equal to 508,208 and $202,005 \text{ m}^3$; based on Eq. (10), the sum of volume is equal to 79,456 and $440,461 \text{ m}^3$; based on Eq. (12), the

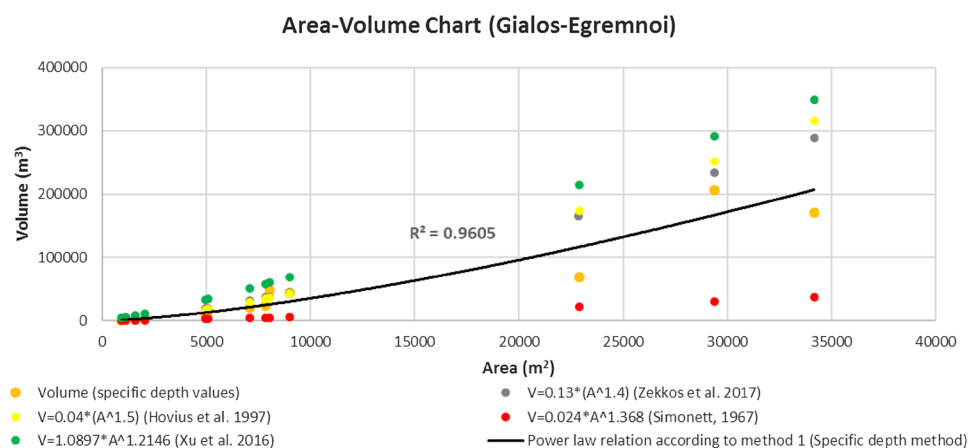
sum of volume is equal to 761,170 and $432,620 \text{ m}^3$; based on Eq. (12), the sum of volume is equal to 596,009 and $252,078 \text{ m}^3$, respectively. It should be mentioned that it was observed by the authors that related to Simonett (1967), a significant underestimation of mean landslide depths was implemented. This concept creates an issue at the volume ranges for each area of interest using the power law equations. Figure 10 shows a visualized perspective of the volume ranges for each region.

The total failure area percentage in Egremnoi region is 41%, and mainly consists of rock slides (17.4%) and secondary of complex slides (6.9%) and deeper slides (6.1%). All the other types of failures (shallow slides, rock slides and rock falls, debris flows, debris flows, and rock falls) result to the 10.4% of the whole area. The total failure area percentage in Gialos area is 26% and mainly consists of complex slides (11.2%) and secondarily of deeper seated slides (9.7%). All the other types of failures (shallow slides, rock slides, rock slides and rock falls, and debris flows) result to the 5.6% of the whole area.

In Figs. 11 and 12 it can be seen that Eq. (9) (Hovius et al. 1997) fits better at our results than Eqs. (10), (11), and (12). According to the relation between the original volume and the volume extracted from Eq. (9), a significant difference occurs in Gialos region on complex slides (the difference is equal to 32%) and in Egremnoi region on rock slides (the difference is equal to 50%). This difference probably relates to the area affected the mentioned failure types (the greatest the percentage of affected area, the greatest the difference of results among each volume estimation method). Another reason could be related to the mean depth of a specific type of landslide (e.g., rock slides or deeper slides).

Moreover, the volumetric results with the mean-depth method are plotted according to the affected area. It became obvious that there is a relation between those data, while a power law function Eq. (15) was constructed which seems to fit well enough with the data ($R^2 = 0.96$). The extracted function is the following, while Fig. 13 shows the plotted

Fig. 13 Volume-to-area relationship based on volume estimation method with specific depth values. The results of Eq. (9) (Hovius et al. 1997), Eq. (10) (Simonett 1967), Eq. (11) (Xu et al. 2016), and Eq. (12) (Zekkos et al. 2017) are also plotted. A power law relation Eq. (15) was constructed regarding only the data originated from this research



pre-mentioned data: with V volume of landslides (m^3) and A area affected by earthquakes (m^2).

$$V = 8.7 \cdot A^{0.67}, \tag{15}$$

with V volume of landslides (m^3) and A area affected by earthquakes (m^2).

Newmark’s analysis

For the purposes of this study, five (5) rasterized parametric layers were developed for the two regions’ case studied, which are relevant to the variables of Eqs. (1) and (2).

In particular, a 5 m-slope raster was created using the 5 m digital terrain model (DTM) grid. Strength parameters per each engineering geological unit were extracted based on the procedure of Hoek–Brown (HB) criteria. As it is previously mentioned, the variables of c' and φ' were evaluated by applying the HB criteria based on the assigned, during the field survey, values of GSI and IRS (σ_{ci}), while the m_i was employed by taking into account data provided by the literature (Hoek 2006).

It has to be underlined that the majority of the researchers used $m=0$ for simplicity reasons or due to arid climate for the studied areas (Jibson et al. 2000; Jibson 2007; Wang and Lin 2010; Papathanassiou 2012; Tang et al. 2013; Chung et al. 2014; Chen et al. 2014; Rodriguez-Peces et al. 2014; Wang et al. 2016; Liu et al. 2017; Vessia et al. 2017), while

Salinas-Jasso et al. (2017) created three models for the three cases that they could be observed ($m=0, m=0.5, m=1$).

The island of Lefkada corresponds to Mediterranean climate, and the rainfalls are quite abundant from mid-September to December. The average monthly rainfall for the months November and December exceeds 1500 mm (Bornovas 1964). However, taking into account that no data regarding the saturation of geological units were available, we decided to be conservative and employed the value $m=0.7$ instead of 1 which is related to saturated conditions.

In Tables 5 and 6, the employed data in Hoek–Brown criterion are listed, to evaluate the friction angle (φ') and cohesive strength (c'). The GSI, σ_{ci} , and H values ranges for each engineering geological unit as it is observed in Tables 5 and 6, and thus, the pre-mentioned values are considered as standard mean values to simplify the calculations. The mean value for slope height was assumed to be equal to 5 m. As a result, for the rock mass, the evaluated friction angle (φ') ranges from 9.4° to 31.4°, while the cohesive strength (c') ranges from 2.8 to 17.7 MPa for Gialos and Egremnoi area.

Regarding the soil material, assumptions were made related to the values of friction angle and cohesive strength according to engineering geological parameters taken from the literature. For loose material, the values are $\varphi=30^\circ$ and $c=0$ KPa in contrast to the cohesive material whose values are $\varphi=30^\circ$ and $c=10$ KPa (Bell 2007).

Table 5 Data used in Hoek–Brown functions to compute friction angle (φ') and cohesion strength (c') of the rock mass for the engineering geological units referring the rock mass, for “Gialos” region

Engineering geological parameters for “Gialos” region								
Engineering geological units	Data					Results		
	A/A	GSI	σ_{ci} (MPa)	m_i	Unit weight γ (KN/m ³)	H (m)	φ' (°)	c' (MPa)
1		70	150	12	25	5	31.4	17.7
2		60	100	10	25	5	24.5	11.8
3		45	50	10	25	5	16.8	6.8
4		20	15	14	25	5	9.4	2.8

Table 6 Data used in Hoek–Brown functions to compute friction angle (φ') and cohesion strength (c') of the rock mass for the engineering geological units referring the rock mass, for “Egremnoi” region

Engineering geological parameters for “Egremnoi” region								
Engineering geological units	Data					Results		
	A/A	GSI	σ_{ci} (MPa)	m_i	Unit weight γ (KN/m ³)	H (m)	φ' (°)	c' (MPa)
1		70	150	12	25	5	31.4	17.7
2		60	100	10	25	5	24.5	11.8
3		45	50	10	25	5	16.8	6.8
4		30	25	14	25	5	12.6	4.4
5		20	15	14	25	5	9.4	2.8

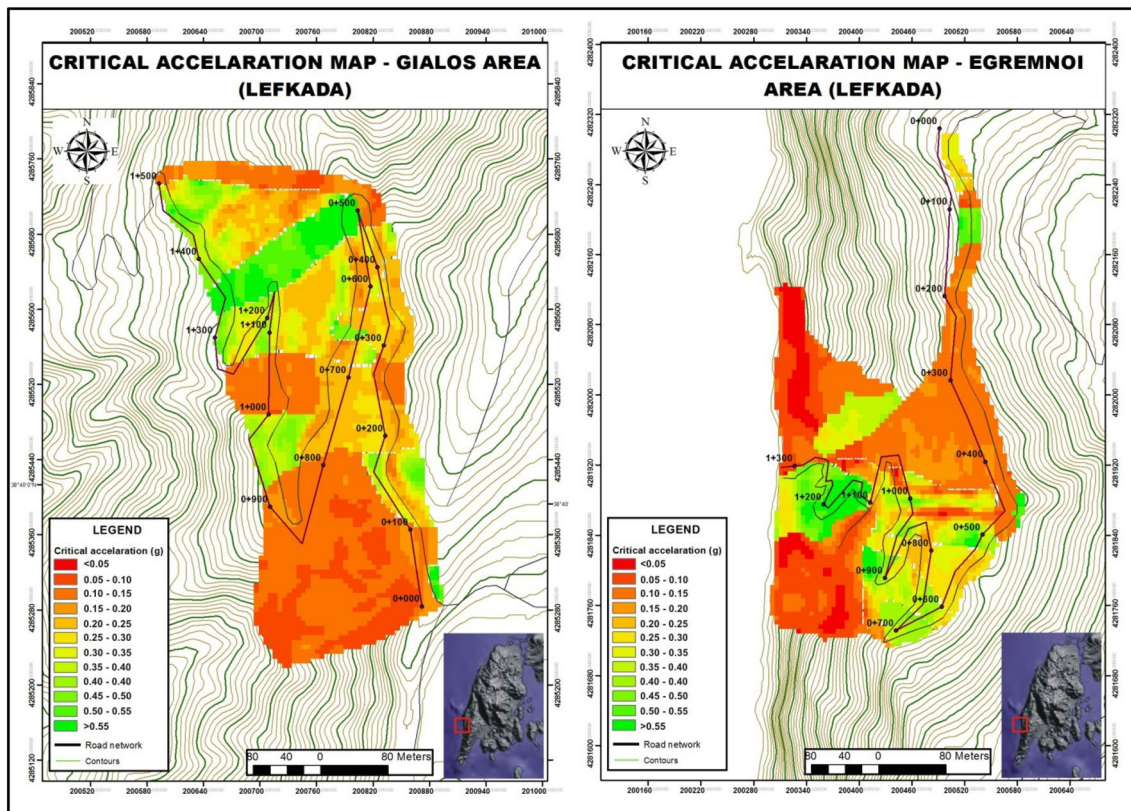


Fig. 14 Critical acceleration maps for Gialos and Egremnoi area

Figure 14 shows two (2) maps according to the susceptibility to seismically triggered landslides in terms of critical acceleration a_c , for each area of interest. The critical acceleration for the most susceptible zones ranges from 0.05 to 0.3 g, while the areas with GSI above 45 are classified at the zones with critical acceleration above 0.55 g. Accordingly, it can be indirectly stated that the PGA value, induced by the 2015 earthquake, at this area should be at least 0.4–0.45 g in order to be capable to trigger landslides.

Discussion

The subject of this study was (a) to evaluate the area (m^2) and volume (m^3) of landslides at the areas of interest and to compare the results with the ones computed based on published relevant equations and (b) the calculation of critical acceleration using Newmark's analysis for the areas of interest.

It is a matter of fact that the landslide mean-depth values that were evaluated by the authors in the present study are quite arguable, while they are based on the literature and by field observation. The total volume area could be fluctuating in a significant range by changing the

considered mean-depth values. An indirect evaluation of the validity of the present method is the comparison of the present's study volume area results with the results extracted from power law equations (area–volume) taken from the literature. The results of the present study seem to correlate quite well with the results extracted from the power law equations. This is an indication that equations constructed from data originated from other world-wide earthquake events could be applied at a different study area in contribution with a validating procedure similar with the procedure followed at the present study.

In the present study, the authors attempt to evaluate the landslide volume results and construct a power law equation which compares the total failure area (m^2) with the total landslide volume (m^3). This equation is observed at Eq. (15), while Fig. 13 shows the power law trendline. It is of major importance that this equation is based on a few data and its reliability is quite considerable. In contrary, the Coefficient of Determination or R^2 value is equal to 0.96 which is an indication of high reliability.

The purpose of this evaluation was to indirectly estimate the value of the strong ground motion, i.e., PGA in these areas. That was achieved by performing a back-analysis based on the spatial distribution of slope failures and the outcome arisen by Newmark's analysis. The regions with

high values of critical acceleration in critical-acceleration maps (Fig. 14) seem to correlate quite well with the actual earthquake-induced landslides (Figs. 6b, 7b) which is an evidence that the critical-acceleration maps are quite qualitative. This procedure could be very important for seismic hazard analysis in countries with scattered strong ground motion network. It is of major importance that these maps must be verified. The verification could be possible with the installation of accelerometers in specific places (especially at the areas with high acceleration values as can be seen at Fig. 14). This kind of verification is time-consuming, since the next earthquake event is compulsory to happen to have realistic results.

Conclusions

In the present study, detailed geological and engineering geological mapping took place. Characterization and perception of rock mass are of major importance to apply methods such as those in the present study. The conclusions of the engineering geological mapping were the following: (a) Gialos region was divided in six (6) engineering geological units [four (4) for limestone bedrock and two (2) for debris material]; (b) Egremnoi region was divided in seven (7) engineering geological units [five (5) for limestone bedrock and two (2) for debris material]; (c) the maximum and minimum Geological Strength Index (GSI) values given in both regions are 60–70 and 15–20, respectively.

In both regions, the main observed failure types are rock slides and combination of rock slides and rock falls. The reason is that the main failure material is limestone breccia with $GSI = 35–45$ or $GSI = 15–20$ which consists of small limestone blocks ($2 \times 2 \times 2$ cm).

The volume's estimation was approached by three different methods. The results of each method seem to correlate well enough as the original method derived from the scientific literature's equations is based on the assumption of mean depths for each type of landslides. In the present study, our results lie closer to the results of Eq. (9) which is proposed by Hovius et al. (1997) as well as it was observed that Eq. (10) (Simonett 1967) significantly underestimates the depths of the landslides in comparison with the other power law equations used in the present study. The results that arisen from this study indicates that, (a) in Gialos region, the landslide area is equal to 26% of the studied area with landslide volume almost equal to $425,000 \text{ m}^3$, while the Deep slides and Complex slides hold 10 and 11% of the total landslide area, respectively; (b) in Egremnoi region, the landslide area is equal to 41% of the studied area with landslide volume almost equal to $193,000 \text{ m}^3$, while the Rock slides hold 17.5% of the total landslide area.

The rasterized engineering geological data (GSI, c , ϕ , and FS) were combined via GIS software and produced results according to the critical acceleration needed for the rock mass or soil to fail. Newmark's analysis is a useful tool to construct critical-acceleration maps which could be used in long-term land-use planning or for maximum fatalities prediction and guidance advice for construction. The conclusion is drawn that the maximum acceleration that it could be measured in the both areas of interest ranges from 0.4 to 0.45 g.

The studied areas (Egremnoi, Gialos) are regions in Lefkada that intensely suffer by seismic events. The November 2015 seismic event led to closure of the roads leading to the coast in both regions due to intense landslide events. The extracted engineering geological information regarding areas with high failure severity could be used by the local community with a view to implemented measures to avoid future landslide phenomena.

Acknowledgements This research was supported by the Aristotle University of Thessaloniki (A.U.TH.) as a master thesis during the period 06/2016–12/2016. Local community is also acknowledged for providing us with helpful information regarding the areas of interest.

References

- Amirahmadi A, Pourhashemi S, Karami M, Akbari E (2016) Modeling of landslide volume estimation. *Open Geosci* 8:360–370
- Barton NR, Lien R, Lunde J (1974) Engineering classification of rock masses for the design of tunnel support. *Rock Mech* 6(4):189–239
- Bell FG (2007) *Engineering geology*. Second Edition. ISBN-13: 978-0-7506-8077-6 ISBN-10: 0-7506-8077-6
- Bieniawski ZT (1989) *Engineering rock mass classifications*. Wiley, New York
- Bornovas I (1964) *Geology of Lefkada Island*. PhD Thesis
- Chen W, Li X, Wang Y, Liu S (2013) Landslide susceptibility mapping using LiDAR and DMC data: a case study in the Three Gorges area, China. *Environ Earth Sci* 70:673–685. <https://doi.org/10.1007/s12665-012-2151-8>
- Chen X-L, Liu C-G, Yu L, Lin C-X (2014) Critical acceleration as a criterion in seismic landslide susceptibility assessment. *Geomorphology* 217:15–22
- Chung J, Rogers J, Watkins C (2014) Estimating severity of seismically induced landslides and lateral spreads using threshold water levels. *Geomorphology* 204:31–41
- Cushing E (1985) *Evolution structurale de la marge nord-ouest hellénique dans l'île de Levkas et ses environs (Greece nord-occidentale)*. PhD Thesis
- Eeckhaut M, Kerle N, Herva's J, Supper R (2013) Cover using object-oriented analysis and LiDAR derivatives. *Landslide Sci Pract*. https://doi.org/10.1007/978-3-642-31325-7_413
- Ganas A, Elias P, Bozionelos G, Papathanassiou G, Avallone A, Papatertgios A, Valkaniotis S, Parcharidis I, Briole P (2016) Coseismic deformation, field observations and seismic fault of the 17 November 2015 $M = 6.5$, Lefkada Island, Greece earthquake. *Tectonophysics* 687:210–222
- Hack R, Huisman M (2002) Estimating the intact rock strength of a rock mass by simple means. *Eng Geol Dev Countries*. In:

- Proceedings of 9th congress of the International Association for Engineering Geology and the Environment. Durban, South Africa, 16–20 Sept 2002, pp 1971–1977
- Harp E, Jibson R (1995) Seismic instrumentation of landslides: building a better model of dynamic landslide behavior. *Bull Seismol Soc Am* 85(1):93–99
- Harp E, Jibson R (2002) Anomalous concentrations of seismically triggered rock falls in Pacoima canyon: are they caused by highly susceptible slopes or local amplification of seismic shaking? *Bull Seismol Soc Am* 92:3180–3189. <https://doi.org/10.1785/0120010171>
- Harp E, Keefer DK, Sato HP, Yagi H (2011) Landslide inventories: the essential part of seismic hazard analyses. *Eng Geol* 122(1–2):9–21
- Harp E, Jibson R, Dart R (2013) The effect of complex fault rupture on the distribution of landslides triggered by the 12 January 2010, Haiti Earthquake. *Landslide Sci Pract* 625(5):157–161
- Harp E, Hartzell S, Jibson R, Ramirez-Guzman L, Schmitt R (2014) Relation of landslides triggered by the kiholo bay earthquake to modeled ground motion. *Bull Seismol Soc Am* 104(5):2529–2540. <https://doi.org/10.1785/0120140047>
- Hasegawa S, Nonomura A, Uchida J, Kawato K, Kageura R, Chiba T, Onoda S (2015) Hazard mapping of earthquake-induced deep-seated catastrophic landslides along the median tectonic line in shikoku by using LiDAR DEM and airborne resistivity data. *Eng Geol Soc Territ*. https://doi.org/10.1007/978-3-319-09057-3_120
- Havenith HB, Torgoev A, Braun A, Schlögel R, Micu M (2016) A new classification of earthquake-induced landslide event sizes based on seismotectonic, topographic, climatic and geologic factors. *Geoenviron Disasters*. <https://doi.org/10.1186/s40677-016-0041-1>
- Hoek E (2006) Practical rock engineering. <https://www.rocscience.com/learning/hoek-s-corner>
- Hovius N, Stark CP, Allen PA (1997) Sediment flux from a mountain belt derived by landslide mapping. *Geology* 25:231–234
- ISRM (1981) Rock characterization, testing and monitoring. In: Brown ET (ed) ISRM suggested methods. Pergamon Press, Oxford, p 211
- ITSAK (2015) Preliminary results of the earthquake M6.4 of 17/11/2015. <http://www.itsak.gr>
- Jaafari A (2018) LiDARsupported prediction of slope failures using an integrated ensemble weightsofevidence and analytical hierarchy process. *Environ Earth Sci* 77:42. <https://doi.org/10.1007/s12665-017-7207-3>
- Jibson R (2007) Regression models for estimating coseismic landslide displacement. *Eng Geol* 91:209–218
- Jibson R, Harp E, Michael J (1998) A method for producing digital probabilistic seismic landslide hazard maps: an example from the Los Angeles, California Area. US Geological Survey Open-File Report, pp 98–113 (17 pp)
- Jibson R, Harp E, Michael J (2000) A method for producing digital probabilistic seismic landslide hazard maps. *Eng Geol* 58:271–289
- Keefer D (1984) Landslides caused by earthquakes. *Geol Soc Am Bull* 95:406–421
- Keefer D (2002) Investigating landslides caused by earthquakes—a historical review. *Surv Geophys* 23:473. <https://doi.org/10.1023/A:1021274710840>
- Lekkas E, Mavroulis S, Alexoudi V (2016) Field observations of the 2015 (November 17, Mw 6.4) Lefkas (Ionian Seas, Western Greece) earthquake impact on natural environment and building stock of Lefkas island. *Bull Geol Soc Greece* 50(1):499–510
- Liu J, Shi J, Wang T, Wu S (2017) Seismic landslide hazard assessment in the Tianshui area, China, based on scenario earthquakes. *Bull Eng Geol Env*. <https://doi.org/10.1007/s10064-016-0998-8>
- Malamud B, Turcotte D, Guzzetti F, Reichenbach P (2004) Landslide inventories and their statistical properties. *Earth Surf Proc Land* 29:687–711
- Marinos V (2010) New proposed GSI classification charts for weak or complex rock masses. *Bull Geol Soc Greece* 4(3):1248–1258
- Marinos P, Hoek E (2000) Predicting tunnel squeezing problems in weak heterogeneous rock masses. *Tunnel Tunnell Int*
- Miles SB, Keefer DK (2000) Evaluation of seismic slope-performance models using a regional case study. *Environ Eng Geosci* 6(1):25–39
- Miyagi T, Yamashina Sh, Esaka F, Abe S (2011) Massive landslide triggered by 2008 Iwate–Miyagi inland earthquake in the Aratozawa Dam area. *Tohoku Jpn Landslides* 8:99–108
- Mountrakis D (2010) Geology and geotectonic evolution of Greece. Univeristy studio Press, pp 207 (ISBN 978-960-12-1970-7)
- Newmark NM (1965) Effects of earthquakes on dams and embankments. *Geotechnique* 15:139–160
- Ohmori H, Hirano M (1988) Magnitude, frequency and geomorphological significance of rocky mud flows, landcreep and the collapse of steep slopes. *Zeitschrift fur Geomorphology (Suppl Bd)* 67:55–65
- Papadopoulos GA, Plessa A (2000) Magnitude–distance relations for earthquake–induced landslides in Greece. *Eng Geol* 58:377–386
- Papathanassiou G (2012) Estimating slope failure potential in an earthquake prone area: a case study at Skolis Mountain, NW Peloponnese, Greece. *Bull Eng Geol Env* 71:187–194. <https://doi.org/10.1007/s10064-010-0344-5>
- Papathanassiou G, Pavlides S, Ganas A (2005) The 2003 Lefkada earthquake: field observations and preliminary microzonation map based on liquefaction potential index for the town of Lefkada. *Eng Geol* 82:12–31
- Papathanassiou G, Valkaniotis S, Dimaras K (2015) Validating the classification of earthquake-induced landslide hazard levels based on data provided by large scale mapping of failures induced by 2003 Lefkada, Greece Earthquake. *Eng Geol Soc Territory* 2:737–741
- Papathanassiou G, Valkaniotis S, Ganas A, Grendas N, Kollia El (2017) The November 17th, 2015 Lefkada (Greece) strike-slip earthquake: Field mapping of generated failures and assessment of macroseismic intensity ESI-07. *Eng Geol* 220:13–30. <https://doi.org/10.1016/j.enggeo.2017.01.019>
- Papazachos BC, Comninakis PE, Karakaisis GF, Karakostas BG, Pappoianou ChA, Papazachos CB, Scordilis EM (2000) A catalogue of earthquakes in Greece and surrounding area for the period 550BC–1999. *Publ Geoph Lab Univ of Thessaloniki*. pp 333
- Pelletier JD, Malamud BD, Blodgett T, Turcotte DL (1997) Scale-invariance of soil moisture variability and its implications for the frequency-size distribution of landslides. *Eng Geol* 48:255–268
- Rodriguez-Peces MJ, Garcia-Mayordomo J, Azanon JM, Jabaloy A (2014) GIS application for regional assessment of seismically induced slope failures in the Sierra Nevada Range, South Spain, along the Padul Fault. *Environ Earth Sci* 72:2423–2435. <https://doi.org/10.1007/s12665-014-3151-7>
- Rondoyanni Th, Sakellariou M, Baskoutas J, Christodoulou N (2012) Evaluation of active faulting and earthquake secondary effects in Lefkada Island, Ionian Sea, Greece: an overview. *Nat Hazards* 61:843. <https://doi.org/10.1007/s11069-011-0080-6>
- Salinas-Jasso J, Ramos-Zuñiga L, Montalvo-Arrieta J (2017) Regional landslide hazard assessment from seismically induced displacements in Monterrey Metropolitan area, Northeastern Mexico. *Bull Eng Geol Env*. <https://doi.org/10.1007/s10064-017-1087-3>
- Saroglou H, Asteriou P, Tsiambaos G, Zekkos D, Clark M, Manoussakis J (2017) Investigation of co-seismic Rockfalls During the 2015 Lefkada and 2014 Cephalonia Earthquakes in Greece. 3rd North American Symposium on Landslides, Roanoke, VA, June 4–8, 2017
- Sasaki Y, Abe M, Hirano I (1991) Fractals of slope failure size-number distribution. *J Jpn Soc Eng Geol* 32:1–11
- Shugen L, Bin D, Zhiwu L, Luba J, Shun L, Guozhi W, Wei S (2013) Geological evolution of the longmenshan intracontinental composite orogen and the eastern margin of the Tibetan Plateau. *J Earth Sci* 24(6):874–890. <https://doi.org/10.1007/s12583-013-0391-5>

- Simonett DS (1967) Landslide distribution and earthquakes in the Bewani and Torricelli Mountains, New Guinea. In: Jennings JN, Mabbutt JA (eds) Landform studies from Australia and New Guinea. Cambridge University Press, Cambridge, pp 64–84
- Tang CL, Hu JC, Lin ML, Yuan RM, Cheng CC (2013) The mechanism of the 1941 Tsaoling landslide, Taiwan: insight from a 2D discrete element simulation. *Environ Earth Sci* 70:1005–1019. <https://doi.org/10.1007/s12665-012-2190-1>
- Valkaniotis S, Ganas A, Papathanassiou G, Papanikolaou M (2014) Field observations of geological effects triggered by the January–February 2014 Cephalonia (Ionian Sea, Greece) earthquakes. *Tectonophysics* 630:150–157. <https://doi.org/10.1016/j.tecto.2014.05.012>
- Varnes DJ (1978) Slope movement types and processes. In: Schuster RL, Krizek RJ (eds) Landslides, analysis and control, special report 176: transportation research board. National Academy of Sciences, Washington, DC, pp 11–33
- Ventura G, Vilardo G, Terranova C, Sessa E (2013) 4D monitoring of active landslides by multi-temporal airborne LiDAR data. *Landslide Sci Pract.* https://doi.org/10.1007/978-3-642-31445-2_419
- Vessia G, Pisano L, Tromba G, Parise M (2017) Seismically induced slope instability maps validated at an urban scale by site numerical simulations. *Bull Eng Geol Env* 76:457–476. <https://doi.org/10.1007/s10064-016-0940-0>
- Wang K-L, Lin M-L (2010) Development of shallow seismic landslide potential map based on Newmark's displacement: the case study of Chi-Chi earthquake, Taiwan. *Environ Earth Sci* 60:775–785. <https://doi.org/10.1007/s12665-009-0215-1>
- Wang Y, Song C, Lin Q, Li J (2016) Occurrence probability assessment of earthquake-triggered landslides with Newmark displacement values and logistic regression: the Wenchuan earthquake, China. *Geomorphology* 258:108–119
- Xu C, Xu X, Yao X, Dai F (2014) Three (nearly) complete inventories of landslides triggered by the May 12, 2008 Wenchuan Mw 7.9 earthquake of China and their spatial distribution statistical analysis. *Landslides* 11:441–461
- Xu C, Xu X, Shen L, Yao Q, Tan X, Kang W, Ma S, Wu X, Cai J, Gao M, Li K (2016) Optimized volume models of earthquake-triggered landslides. *Sci Rep* 6:29797. <https://doi.org/10.1038/srep29797>
- Zekkos D, Clark M, Cowell K, Medwedeff W, Manousakis J, Tsiambaos G, Saroglou H (2017) Satellite and UAV-enabled mapping of landslides caused by the November 17th 2015 Mw 6.5 Lefkada earthquake. Proceedings of the 19th International Conference on Soil Mechanics and Geotechnical Engineering, Seoul 2017